 CMES, vol.39, no.3, pp.237-262, 2009

Intensity of stress singularity at a vertex and along the free edges of the interface in 3D-dissimilar material joints using 3D-enriched FEM

W. Attaporn[1] **and H. Koguchi**[2]

Abstract: In the present study, a stress singularity field along free edges meeting at a corner in a three-dimensional joint structure is investigated. The order of stress singularity is determined using an eigen analysis based on a finite element method. Intensities of stress singularity not only at the corner but also along the free edge of interface are determined directly without any post-processing by a new FEM formulation referred to as a three-dimensional enriched FEM. Result in the present analysis is also compared with that in another numerical method. It was slightly larger than the intensity of stress singularity, which was determined by a three-dimensional boundary element method (BEM).

Keywords: Intensity of stress singularity, 3D-enriched FEM, singular point, singularity corner, singularity line.

1 Introduction

Industrial products such as electronic devices and heat endurance parts are composed of dissimilar materials. A mismatch of material properties causes a failure at the free edge of joint because a stress concentration occurs along the free edge of interface especially at the vertex of joint. Consequently, a stress field at a vertex in dissimilar material joints has been investigated using several numerical methods proposed by many authors. The study on this field has been carried out step by step.

Williams (1952) used the mathematical procedure for analyzing stress singularities in infinite wedges and successfully applying to the analysis of stress distribution at the vicinity of a crack tip [Williams (1957)]. Zak and Williams (1963) used eigen functions for analyzing stress singularity field at a crack tip perpendicular to a bi-material interface. They found that a real part of eigen value is within the range

[1] Graduate school of NUT, Nagaoka, Niigata, Japan
[2] NUT, Nagaoka, Niigata, Japan

of 0 to 1, and expressed a relationship between stress distribution and the order of stress singularity at the crack tip. Aksentian (1967) determined eigen values and eigen vectors at the singular point in plane intersecting a free edge of the interface in three-dimensional dissimilar joints. Bogy (1971) and Bogy and Wang (1971) analyzed the plane problem of bonded dissimilar material wedges under a surface traction and determined the stress singularity field at the corner in the wedge. They determined the order of stress singularity depending on material constants and the angle of wedges. Kawai, Fujitani and Kobayashi (1977) performed the stress analysis at a conical surface pit and applied Williams' method to the three-dimensional crack problems. Numerical analysis of characteristic roots for conical pit problem was made for determining eigen values at the vertex of conical pit. Kawai, Fujitani and Kumagai (1977) investigated stress singularity of a three-dimensional surface crack, especially its peculiar behavior at the free end of the crack front line, and then analyzed the surface crack problem by employing spherical coordinates. Benthem (1977, 1980) determined the eigen values using eigen analysis and examined stress components of Cartesian coordinate at the vertex of a quarter-infinite crack in a half-space for various Poisson's ratios.

Bazent and Estenssoro (1979) and Yamada and Okumura (1981) developed a finite element analysis for solving eigen value equation to determine directly the order of stress singularity and the angular variation of the stress and displacement fields. This eigen analysis was used to evaluate the order of singularity at a point where a crack meets a free surface in an isotropic material. Then, this eigen analysis based on a finite element was adapted by Pageau, Joseph and Biggers (1995) to use for analyzing the inplane deformation of wedges and junctions composed of anisotropic materials. The stress and displacement fields were obtained from eigen formulation for real and complex orders of stress singularity. Pageau and Biggers (1995) applied to analyze the joints including fully bonded multi-material junctions intersecting a free edge as well as materials containing crack intersecting a free edge. This study showed that the order of singularity in the three-dimensional stress field could be accurately determined with a relatively small number of elements. Pageau and Biggers (1996) determined the order of stress singularity and the angular variation of the displacement and the stress fields around the singular points in plane intersecting a wedge front in the three-dimensional anisotropic material structures using the two-dimensional displacement formulation under a plane strain assumption.

Koguchi (1996) examined the order of stress singularity at vertex and also along the stress singularity line between two isotropic materials in joints using eigen analysis. The stress distributions around the vertex were determined using a boundary element method (BEM). Koguchi (2006) determined the intensity of singularity

by fitting the stress profile that obtained from BEM analysis with a least square method.

Leblond and Leguillon (1999) examined the asymptotic behavior of the stress intensity factors near an angular point of a crack front in homogeneous isotropic elastic body in the cases of the crack presents a notch or a corner.

Dimitov, Andra and Schnake (2001, 2002) presented the three-dimensional eigen analysis which was solved iteratively using Arnoldi method. This method needs only the small banded matrix when compared with normally used determinant method. The order of singularities at corners and free edges of the interface in laminate composite material joints were determined using the eigen analysis.

Lee and Im (2003) used a two-state M-integral for computing the near-tip stress intensities around three-dimensional wedges and used an eigen analysis for determining eigen values and eigen vectors.

Apel, Leguillon, Pester and Yosibash (2008) determined edge singularity by the use of three-dimensional Williams' expansion. The edge stress intensity factors along the reentrant wedge front were determined using a quasi-dual function method. Omer and Yosibash (2008) and Yosibash, Omer and Dauge (2008) computed the complex eigen function by using a p-version finite element method and examined the edge stress intensity factors at the edge vicinity in three-dimensional anisotropic multi-material interfaces using a quasi-dual function method.

From the above, many authors individually determined the intensities of singularity at a corner singular point or along the free edges of the interface in a three-dimensional dissimilar material joint.

However, the intensity of singularity should be considered at the singularity corner together with that along the free edge of the interface in a three-dimensional material joint.

The normal use of a standard finite element analysis is hard to analyze a stress field at a singular point in a real dissimilar material joint. It is very difficult to determine the intensity of stress singularity by fitting the three-dimensional stress profile with a least square method. Moreover, an extremely large number of element and much calculation time are required for determining three-dimensional stress profiles around a singular point.

To reduce the number of element and the calculation time, many authors have developed element-free methods which can be simply called as meshless methods. Nayroles, Touzot and Villon (1992) proposed the diffuse element method. Belytschko, Lu and Gu (1994) presented the element–free Galerkin method (EFGM). Later, Atluri and Zhu (1998) originated the meshless local Petrov-Galerkin (MLPG). The MLPG method is truly meshless method as no meshes are required either for inter-

polation purposes or for integration proposes. Then, Atluri and Zhu (2000) applied the MLPG methods to solve the elasto-static problems. Furthermore, the various researches of MLPG method were given by Atluri and his colleagues such as Atluri and Shen (2002); Atluri, Han and Shen (2003); Atluri (2004a); Atluri, Han and Rajendran (2004b); Atluri, Lui and Han (2005); Atluri, Lui and Han (2006). The MLPG for three-dimensional elasto-static is developed by Li, Shen, Han and Atluri (2003) and for the problem of topology-optimization of elastic structures is developed by Li and Atluri (2008).

Hagihara, Tsunori, Ikeda and Miyazaki (2007) proposed the elastic-plastic EFGM to determine the fields of displacement, strain and stress for a crack problem, and calculated the elastic- plastic fracture mechanics parameters (J-integral and T^*-integral). Nie, Chang and Fan (2007) presented a high performance parallel seamless connection between the FEM mesh generation process and the FEM structure analysis process for a new node-based seamless finite element method. Wen, Aliabadi and Liu (2008) introduced the EFGM with enriched radial base functions for determining the stress singularity at a crack tip.

A kind of meshless FEM namely enriched FEM for three-dimensional joints is presented in this study. The new enriched FEM formulation is extended the enriched FEM formulation in the papers of Benzley (1974) and Pageau and Biggers (1997) to determine the intensities of stress singularity at a singularity corner together with those along the free edge of the interface in three-dimensional dissimilar material joints. The papers of Benzley (1974) and Pageau and Biggers (1997) are briefly explained later. Recently, the enriched FEM has gained much attention from many authors. Wen-Hwa Chen and Cheng-Hung Chen (2005) developed the enriched meshless method using meshless interpolations and a global Galerkin approach for the analysis of three-dimensional fracture problems.

Ayhan and Nied (2002) used the enriched FEM to determine stress intensity factors along the crack front except at the singular point where the crack front intersects the free surface. Ayhan, Kaya and Nied (2006) applied the enrich FEM for the analysis of three-dimensional interface crack in the dissimilar material structures. Later, Ayhan (2007, 2009) developed the three-dimensional enriched FEM to compute the stress intensity factors (2007) and the mixed-mode stress intensity factors (2009) for three-dimensional cracks contained in functionally graded materials (FGMs).

The three-dimensional enriched FEM formulation for determining the intensity of stress singularity at a corner singular point is not expressed until now. Therefore, the intensities of stress singularity at the corner and also along the free edge of interface are directly determined by this method without any post-processing.

2 Formulation of 3D-enriched FEM

A traditional FEM is generally used for investigating unknown displacements at each node in a FEM model. The displacement can be expressed using a hexahedron element as

$$u_i = \sum_{n=1}^{8} N_n \bar{u}_{in}, \tag{1}$$

where N_n is the standard interpolation function associated with node n and $\bar{u}_{in}$ is nodal displacement at node n for direction i (i= 1, 2 and 3 are x, y and z directions, respectively).

For the enriched FEM, Benzley (1974) expressed the displacement function of two-dimensional enriched FEM for determining the stress intensity factors in two-dimensional structures including a crack tip. See Eq. 2.

$$u_i = \sum_{n=1}^{4} N_n \bar{u}_{in} + K_I Q_{iI}(r,\theta) + K_{II} Q_{iII}(r,\theta) \tag{2}$$

In equation 2, Q_{iI} and Q_{iII} are the asymptotic mode I and mode II crack tip displacement functions in polar coordinates (r, θ), K_I and K_{II} are the stress intensity factors of mode I and mode II, respectively. The arbitrary Benzley's quadrilateral element with a singular point S is shown in Fig. 1.

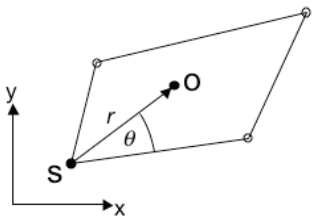

Figure 1: A quadrilateral element with a singular point

Pageau and Biggers (1995) determined the asymptotic displacement function in cylindrical coordinates along a wedge front using eigen analysis. Pageau and Biggers (1997) further created the enriched element formulation for determining stress intensity factors along a wedge front in solid structures with wedge configurations and multi-material junctions.

In this paper, the intensities of singularity are determined along the free edges meeting at a vertex. Figure 2 shows the location of points O in spherical and cylindrical

coordinates, which are located for expressing displacement fields around the singular points at the corner and along singularity lines, respectively.

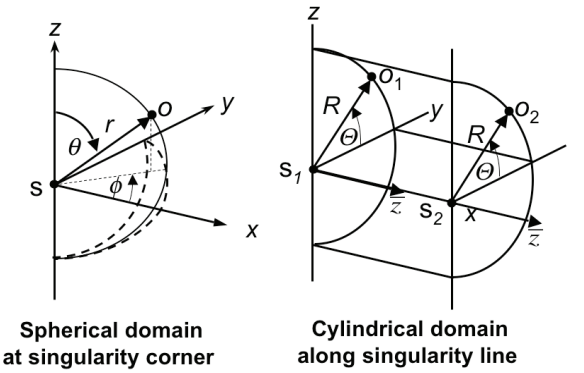

Figure 2: The location of points O in spherical (left) and cylindrical (right) coordinates

The displacement formulation including the asymptotic displacement terms around the singular points along the free edges meeting at a vertex is expressed using a hexahedron element as the following equation.

$$u_i = \sum_{n=1}^{8} N_n \bar{u}_{in} + \sum_{j=1}^{J} K_{ij}^{c} \, \mathcal{Q}_{ij}^{c}(r,\theta,\phi) + \sum_{j=1}^{J} \left[\sum_{m=1}^{M_X} \left\{ \tilde{N}_m^{lx} K_{ijm}^{lx} \, \mathcal{Q}_{ij}^{lx}(R,\Theta,\bar{z}) \right\} \right] + \sum_{j=1}^{J} \left[\sum_{m=1}^{M_Y} \left\{ \tilde{N}_m^{ly} K_{ijm}^{ly} \, \mathcal{Q}_{ij}^{ly}(R,\Theta,\bar{z}) \right\} \right] \tag{3}$$

In equation 3, J represents the number of eigen value, p_j, obtained from eigen analysis. M_X and M_Y are the number of singularity points along the singularity lines in x axis (singularity line x, lx) and y axis (singularity line y, ly), respectively. $\tilde{N}_m^{lx}$ and $\tilde{N}_m^{ly}$ are the standard interpolation functions of a 2-node linear element along the singularity lines x and y, respectively. Then the asymptotic displacement

field terms are expressed as

$$\begin{aligned}
\mathcal{Q}_{ij}^{c}(r,\theta,\phi) &= Q_{ij}^{c}(r,\theta,\phi) - \sum_{a=1^{st}ec}^{Last\,ec} N_a \bar{Q}_{ija}^{c}(r,\theta,\phi), \\
\mathcal{Q}_{ij}^{lx}(R,\Theta,\bar{z}) &= Q_{ij}^{lx}(R,\Theta,\bar{z}) - \sum_{a=1^{st}elx}^{Last\,elx} N_a \bar{Q}_{ija}^{lx}(R,\Theta,\bar{z}), \\
\mathcal{Q}_{ij}^{ly}(R,\Theta,\bar{z}) &= Q_{ij}^{ly}(R,\Theta,\bar{z}) - \sum_{a=1^{st}ely}^{Last\,ely} N_a \bar{Q}_{ija}^{ly}(R,\Theta,\bar{z}).
\end{aligned} \tag{4}$$

Where Q_{ij}^{c}, Q_{ij}^{lx} and Q_{ij}^{ly} represent the asymptotic displacement fields in the direction i at corner (c), singularity lines x and y, respectively. Then, $\bar{Q}_{ija}^{c}$, $\bar{Q}_{ija}^{lx}$ and $\bar{Q}_{ija}^{ly}$ are the asymptotic displacement fields at node a which is taken by the assumption of singularity domains. An a can be a number of node in a hexahedron element (1 to 8) depends on the 3 lists of node numbers; the lists of the singularity corner domain (*ec*), the singularity line domains (*elx* and *ely*) associated with x and y axes, respectively. The example of the list of singularity enriched domains is shown in Fig. 3. N_a is the standard interpolation function of the node a in a hexahedron element.

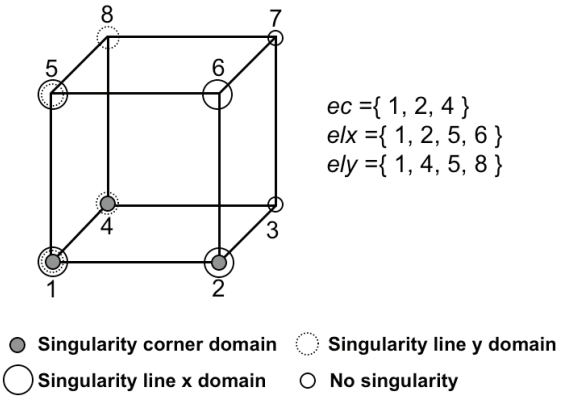

Figure 3: The list of singularity enriched domains (example)

2.1 Numerical singular displacement field

The angular variation of displacements and the eigen values could be determined by finite element formulation using an interpolation function [Yamada and Okumura (1981), Pageau and Biggers (1995)]. Figure 4 shows a definition of the finite

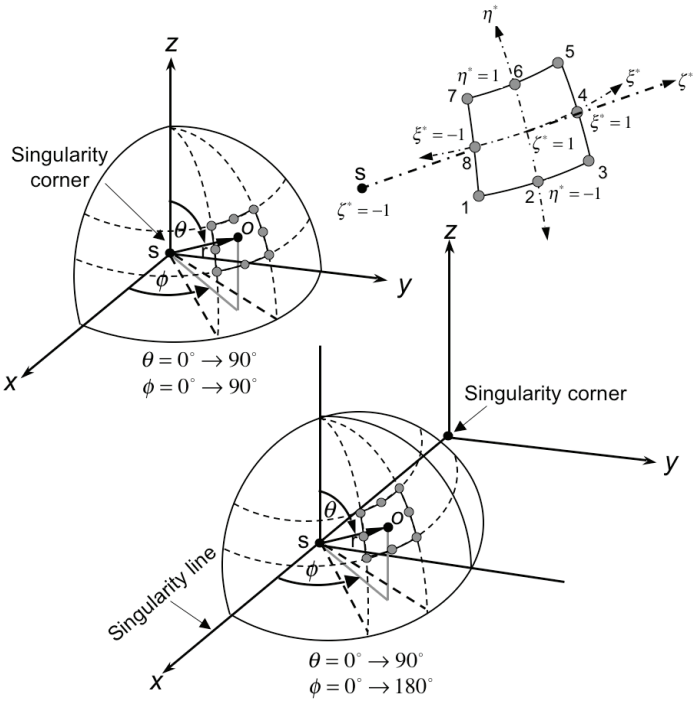

Figure 4: Definition of the finite element geometry for eigen analysis in spherical coordinates

element geometry for eigen analysis in spherical coordinates at the singularity corner and along the singularity line where a singular stress state occurs at point S. The spherical domain surrounding the singular point is divided into 8-node quadrilateral elements. A point O is located in an element. The location of point O in spherical coordinate can be expressed as

$$r = \rho r_0 = r_0 \left(\frac{1+\zeta^*}{2} \right)^{\frac{1}{p}}, \quad \theta = \sum_{n=1}^{8} H_n \theta_n, \quad \phi = \sum_{n=1}^{8} H_n \phi_n. \tag{5}$$

The interpolation functions of an 8-node quadrilateral elements at nodes n are expressed as the following equations.

When n is located at the corner nodes in the element,

$$H_n = \frac{1}{4}(1+\xi_n^*\xi^*)(1+\eta_n^*\eta^*)(\xi_n^*\xi^* + \eta_n^*\eta^* - 1). \tag{6}$$

When n is located at the middle nodes which ξ_n^* is zero in the element,

$$H_n = \frac{1}{2}\left(1-\xi^{*2}\right)\left(1+\eta_n^*\eta^*\right). \tag{7}$$

When n is located at the middle nodes which η_n^* is zero in the element,

$$H_n = \frac{1}{2}\left(1+\xi_n^*\xi^*\right)\left(1-\eta^*\right). \tag{8}$$

Where ξ^*, η^* and ζ^* are the natural coordinates of element whose ranges are defined as shown in Fig. 4.

The displacement at the singular point is taken as zero and the displacement fields around the singular point in i-directions are assumed to be of Eq. 9.

$$\left\{u_j^*\right\} = \left(\frac{r}{r_0}\right)^{p_j}\left\{f_j(\theta,\phi)\right\} \tag{9}$$

Where

$$\left\{f_j(\theta,\phi)\right\} = \sum_{n=1}^{8} H_n\left(\xi^*,\eta^*,\zeta^*\right)\left\{\bar{u}_{nj}^*\right\} \tag{10}$$

Angles θ and ϕ in the spherical coordinates are expressed using the interpolation functions as follows:

$$\theta = \sum_{n=1}^{8} H_n\left(\xi^*,\eta^*,\zeta^*\right)\{\theta_n\}, \quad \phi = \sum_{n=1}^{8} H_n\left(\xi^*,\eta^*,\zeta^*\right)\{\phi_n\} \tag{11}$$

Then, the eigen equation is derived by principles of virtual work for deducing the root p_j.

$$\left(p^2\left[\tilde{A}\right] + p\left[\tilde{B}\right] + \left[\tilde{C}\right]\right)\{U\} = 0 \tag{12}$$

Where $\left[\tilde{A}\right]$, $\left[\tilde{B}\right]$ and $\left[\tilde{C}\right]$ are matrices consisting of elastic modulus matrix [C] and differential operator matrix [B]. $\{U\}$ is the displacement vector. There are a lot of root p that related to the order of singularity$(\lambda, \lambda = 1-p)$, obtained from solving the characteristic equation.

Here, the angular variation of displacements $\left(\bar{u}_{rnj}^*, \bar{u}_{\theta nj}^*, \bar{u}_{\phi nj}^*\right)$ can be derived by eigen analysis. After that, the asymptotic displacement function around the singularity corner $\bar{Q}_{ija}^c$ in Eq. 4 is directly calculated by the eigen vectors $\left(\bar{u}_{rnj}^*, \bar{u}_{\theta nj}^*, \bar{u}_{\phi nj}^*\right)$ in spherical coordinates and then converted to Cartesian coordinates as Eq. 16.

However, to express the continuous singularity fields along the singularity lines, only the cross section of the spherical domain at $\phi = \pi/2$ is considered. The three-dimensional eigen vectors $\left(\bar{u}^*_{rnj}, \bar{u}^*_{\theta nj}, \bar{u}^*_{\phi nj}\right)$ around the singular points of this cross section are converted to the three-dimensional eigen vectors $\left(\bar{u}^*_{Rnj}, \bar{u}^*_{\Theta nj}, \bar{u}^*_{\bar{z}nj}\right)$ in cylindrical coordinates as follows:

$$\begin{Bmatrix} \bar{u}^*_{Rnj} \\ \bar{u}^*_{\Theta nj} \\ \bar{u}^*_{\bar{z}nj} \end{Bmatrix} = [A]^{-1}[F] \begin{Bmatrix} \bar{u}^*_{rnj} \\ \bar{u}^*_{\theta nj} \\ \bar{u}^*_{\phi nj} \end{Bmatrix} \tag{13}$$

Where

$$[A]^{-1} = \begin{bmatrix} 0 & \cos(\Theta) & \sin(\Theta) \\ 0 & -\sin(\Theta) & \cos(\Theta) \\ 1 & 0 & 0 \end{bmatrix} \tag{14}$$

$$[F] = \begin{bmatrix} \sin(\theta)\cos(\phi) & \cos(\theta)\cos(\phi) & -\sin(\phi) \\ \sin(\theta)\sin(\phi) & \cos(\theta)\sin(\phi) & \cos(\phi) \\ \cos(\theta) & -\sin(\theta) & 0 \end{bmatrix} \tag{15}$$

Hence, the elements around the singular point of this cross section become the 3-node linear elements as shown in Fig. 5.

Then the asymptotic displacement functions $\bar{Q}^{lx}_{ija}$ and $\bar{Q}^{ly}_{ija}$ along the singularity lines are calculated by using the displacements $\left(\bar{u}^*_{Rnj}, \bar{u}^*_{\Theta nj}, \bar{u}^*_{\bar{z}nj}\right)$ and then converted to Cartesian coordinates as Eq. 17.

The asymptotic displacement functions $\bar{Q}^{c}_{ija}$, $\bar{Q}^{lx}_{ija}$ and $\bar{Q}^{ly}_{ija}$ in Cartesian coordinates are expressed as the following equations.

$$\begin{aligned}
Q^c_{xj} &= \left(\frac{r}{L}\right)^{p^{sc}_j} \left(\left[\sum_{n=1}^{8} H^{sc}_n \bar{u}^*_{rnj}\right] \sin(\theta)\cos(\phi) - \left[\sum_{n=1}^{8} H^{sc}_n \bar{u}^*_{\phi nj}\right] \sin(\phi) \right. \\
&\quad \left. + \left[\sum_{n=1}^{8} H^{sc}_n \bar{u}^*_{\theta nj}\right] \cos(\theta)\cos(\phi) \right) \\
Q^c_{yj} &= \left(\frac{r}{L}\right)^{p^{sc}_j} \left(\left[\sum_{n=1}^{8} H^{sc}_n \bar{u}^*_{rnj}\right] \sin(\theta)\sin(\phi) + \left[\sum_{n=1}^{8} H^{sc}_n \bar{u}^*_{\phi nj}\right] \cos(\phi) \right. \\
&\quad \left. + \left[\sum_{n=1}^{8} H^{sc}_n \bar{u}^*_{\theta nj}\right] \cos(\theta)\sin(\phi) \right) \\
Q^c_{zj} &= \left(\frac{r}{L}\right)^{p^{sc}_j} \left(\left[\sum_{n=1}^{8} H^{sc}_n \bar{u}^*_{rnj}\right] \cos(\theta) - \left[\sum_{n=1}^{8} H^{sc}_n \bar{u}^*_{\theta nj}\right] \sin(\theta) \right)
\end{aligned} \tag{16}$$

And

$$
\begin{aligned}
Q_{xj}^{lx} = Q_{yj}^{ly} &= \left(\frac{R}{L}\right)^{p_j^{sl}} \left(\left[\sum_{n=1}^{3} H_n^{sl} \bar{u}_{Rnj}^{*} \right] \cos(\Theta) - \left[\sum_{n=1}^{3} H_n^{sl} \bar{u}_{\Theta nj}^{*} \right] \sin(\Theta) \right) \\
Q_{yj}^{lx} = Q_{xj}^{ly} &= \left(\frac{R}{L}\right)^{p_j^{sl}} \left(\left[\sum_{n=1}^{3} H_n^{sl} \bar{u}_{Rnj}^{*} \right] \sin(\Theta) + \left[\sum_{n=1}^{3} H_n^{sl} \bar{u}_{\Theta nj}^{*} \right] \cos(\Theta) \right) \\
Q_{zj}^{lx} = Q_{zj}^{ly} &= \left(\frac{R}{L}\right)^{p_j^{sl}} \left(\left[\sum_{n=1}^{3} H_n^{sl} \bar{u}_{\bar{z}nj}^{*} \right] \right)
\end{aligned}
\tag{17}
$$

Here, the radius r at the singularity corner and the radius R at the singularity point along the singularity line are expressed as

$$r = \sqrt{\left(x - x_S^c\right)^2 + \left(y - y_S^c\right)^2 + \left(z - z_S^c\right)^2}, \tag{18}$$

$$R = R^{lx} \sqrt{\left(y - y_S^{lx}\right)^2 + \left(z - z_S^{lx}\right)^2} \tag{19}$$

where the singular point is on the singularity line in x-axis and

$$R = R^{ly} \sqrt{\left(x - x_S^{ly}\right)^2 + \left(z - z_S^{ly}\right)^2} \tag{20}$$

where the singular point is on the singularity line in y-axis.

An integration point in the FEM analysis is located at (x, y, z) in Cartesian coordinates. The singularity corner is located at the point S of (x_S^c, y_S^c, z_S^c). The singular points along the singularity lines x and y are located at (x_S^{lx}, y_S^{lx}, z_S^{lx}) and (x_S^{ly}, y_S^{ly},z_S^{ly}), respectively.

Then, the angles θ, ϕ and θ are expressed as following equations.

$$\theta = \frac{\pi}{2} \pm \tan^{-1}\left(\frac{\left|z - z_S^c\right|}{r}\right) \tag{21}$$

The angle θ is smaller than $\pi/2$ when the point O is higher than the singular point in z-direction and larger than $\pi/2$ when the point O is lower than the singular point in z-direction.

$$\phi = \tan^{-1}\left(\frac{y - y_S^c}{x - x_S^c}\right) \tag{22}$$

When the singular point is located on the singularity line x,

$$\Theta = \tan^{-1}\left(\frac{z - z_S^{lx}}{y - y_S^{lx}}\right). \tag{23}$$

When the singular point is located on the singularity line y,

$$\Theta = \tan^{-1}\left(\frac{z - z_S^{ly}}{x - x_S^{ly}}\right). \tag{24}$$

The interpolation function, H_n is composed of the interpolation function H_n^{sc} of spherical domain element around the singularity corner and the interpolation function H_n^{sl} of cylindrical domain element around the singular points along the singularity lines. Firstly, the formulations of H_n^{sc} are in the form of Eqs. 6 to 8 but the natural coordinate parameters ξ^* and η^* are replaced by $\hat{\xi}$ and $\hat{\eta}$ that obtained from the location of angle θ and ϕ as the following equation.

$$\hat{\xi} = \frac{2(\phi - \phi_2)}{\phi_d}, \hat{\eta} = \frac{2(\theta - \theta_8)}{\theta_d} \tag{25}$$

Where $\phi_d = \phi_3 - \phi_1$ and $\theta_d = \theta_5 - \theta_3$.

At last, the formulations H_n^{sl} of the 3-node linear element in Fig. 5 are

$$H_1^{sl} = \frac{1}{2}\left(-\hat{\eta} + \hat{\eta}^2\right), \quad H_2^{sl} = 1 - \hat{\eta}^2, \quad H_3^{sl} = \frac{1}{2}\left(\hat{\eta} + \hat{\eta}^2\right) \tag{26}$$

where $\hat{\eta} = \frac{2(\Theta - \Theta_2)}{\theta_d}$ and $\Theta_d = \Theta_3 - \Theta_1$.

2.2 Singularity enriched domain

The influence of singular stress state is considered in the three-dimensional enriched FEM and represented by the asymptotic displacement fields in each element. It is called that "three-dimensional enriched domain". The enriched domains are composed of the singularity corner domain, the singularity line x and y domains as shown in Fig. 6. It has many types of element associated with the three-dimensional enriched domains. The FEM models with the various sizes of the three-dimensional enriched domains are analyzed using the three-dimensional enriched FEM.

3 FEM model and boundary conditions

Generally, dissimilar material tensile block as shown in Fig. 7 can be used as a standard numerical model to investigate the characteristics of stress field and compare the numerical results with other methods of many researchers. In the present study, the case of a large difference of Young's moduli is considered and the three-dimensional dissimilar material joint is subjected to a uniform tensile stress σ. The joint structure is symmetrical in x=10 and y=10 planes. An upper half model of a symmetrical structure is analyzed using a three-dimensional enriched

FEM. The FEM model and boundary conditions are shown in Fig. 8. The small elements are arranged near the corner and singularity lines.

A uniform tensile stress is applied on upper side of FEM model in the z-direction. The FEM model is fixed in the x-direction on the right side, fixed in the y-direction on the back and fixed in the z-direction at the bottom of the model. The material properties with the large difference of Young's moduli dissimilar material joint are shown in the table 1. The upper material (material 1) is hard and the lower material (material 2) is soft.

Table 1: Material properties

Material	E(GPa)	ν
1	215	0.28
2	2.97	0.38

4 Eigen analysis results

In this analysis, first of all, eigen values and eigen vectors are investigated by eigen analysis when two different materials are bonded. The eigen analysis models are subdivided to 8-node quadrilateral elements in division of angles θ and ϕ are $\pi/18$ as shown in Fig. 4. Solving Eq. 12 yields many roots p_j and eigen vectors corresponding to each eigen value are obtained. However, when the root p_j is within the range of $0 < p_j < 1$, the stress field has singularity. The results of eigen value and the order of singularity at the singularity corner and singularity lines points are shown in table 2 and 3.

The subscript j is 1 for the first eigen value which causes a stress singularity in both cases. The angular variations of displacement fields for the eigen values p_j^{sl} and p_j^{sc} which lead to a singular stress state, respectively are shown in Figs. 9 to 10. Then, Eq. 3 has normalized to Eq. 27 so that the singular fields lead to the state which the angular variation of stress components around the singularity corner is one at the angle $\theta = \pi/2$ and $\phi = \pi/4$, $\sigma_{\theta\theta}(\theta = \pi/2) = K_{\theta\theta} r^{-\lambda_j}$.

$$
\begin{aligned}
u_i = &\sum_{n=1}^{8} N_n \bar{u}_{in} + \sum_{j=1}^{J} \frac{K_{ij}^{c}}{E_2} \mathcal{Q}_{ij}^{c}(r,\theta,\phi) + \sum_{j=1}^{J} \left[\sum_{m=1}^{M_X} \left\{ \tilde{N}_m^{lx} \frac{K_{ijm}^{lx}}{E_2} \mathcal{Q}_{ij}^{lx}(R,\Theta,\bar{z}) \right\} \right] \\
&+ \sum_{j=1}^{J} \left[\sum_{m=1}^{M_Y} \left\{ \tilde{N}_m^{ly} \frac{K_{ijm}^{ly}}{E_2} \mathcal{Q}_{ij}^{ly}(R,\Theta,\bar{z}) \right\} \right]
\end{aligned}
\tag{27}
$$

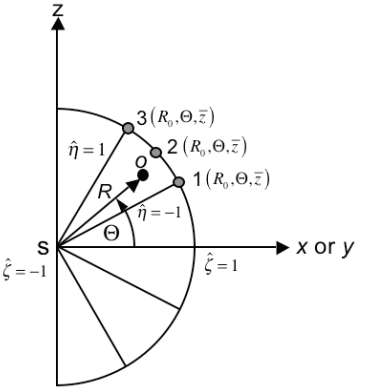

Figure 5: Definition of the finite element geometry for a cross section in cylindrical coordinates

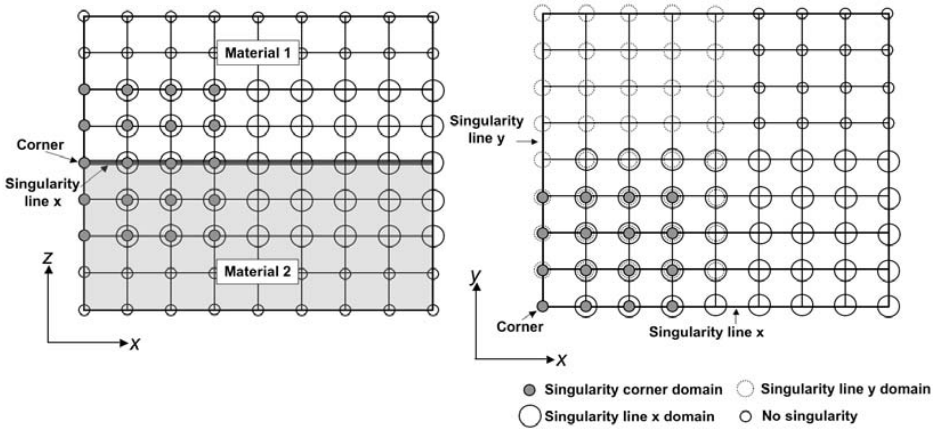

Figure 6: 3D enriched domains in the side view (left) and the interface of dissimilar material joint (right)

5 Boundary element analysis and model

Recently, many researchers have developed numerical methods for determining the intensity of stress singularity in a three-dimensional dissimilar joint. One of them, Koguchi (2006) used a boundary element method (BEM) for determining the intensity of stress singularity fields at a vertex in three-dimensional joints with an interlayer. The stress distributions near the vertex on the boundaries in a Cartesian coordinate are converted to express the inner stress distributions in a spheri-

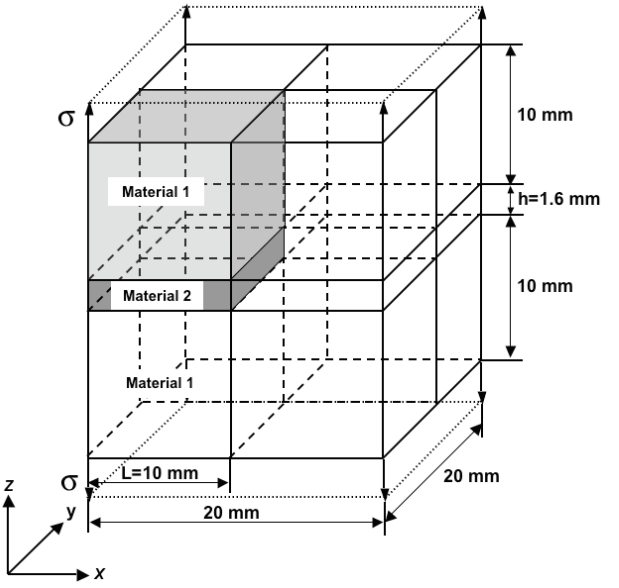

Figure 7: Three-dimensional dissimilar material joint under a uniform tensile stress σ

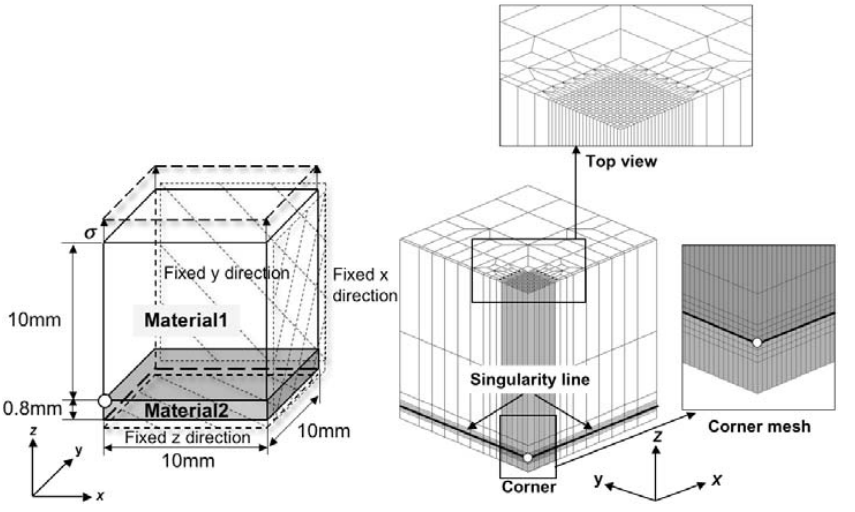

Boundary conditions FEM model

Figure 8: FEM model and boundary connections

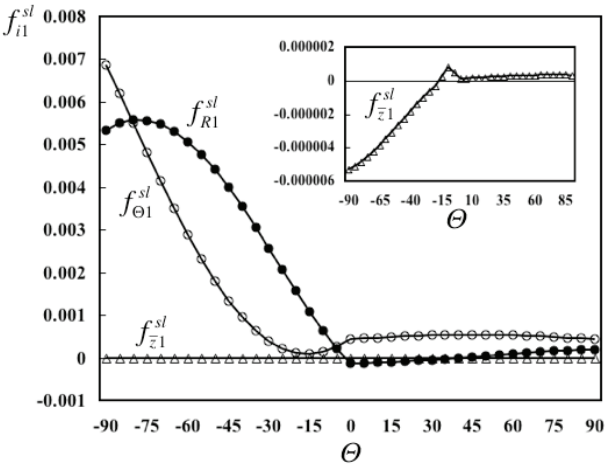

Figure 9: Distribution of angular variation of displacement fields f_{ij}^{sl} in polar coordinates (R, Θ)

Table 2: The order of singularity at a singularity corner

p_j^{sc}		λ_j^{sc}	
Real	Imaginary	Real	Imaginary
0.6018	0.0000	0.3982	0.0000
1.0000	0.0000	0.0000	0.0000
1.0000	0.0000	0.0000	0.0000
1.0000	0.0000	0.0000	0.0000

Table 3: The order of singularity at a singular point along the singularity line

p_j^{sl}		λ_j^{sl}	
Real	Imaginary	Real	Imaginary
0.6786	0.0000	0.3214	0.0000
1.0008	0.0000	-0.0008	0.0000
1.0003	0.0000	-0.0003	0.0000
1.0000	0.0000	0.0000	0.0000
1.0000	0.0000	0.0000	0.0000

cal coordinate. Afterwards, the intensities of stress singularity are determined by fitting stress profiles using a least square method. In the present study, the three-dimensional enriched FEM model, boundary conditions and material properties are

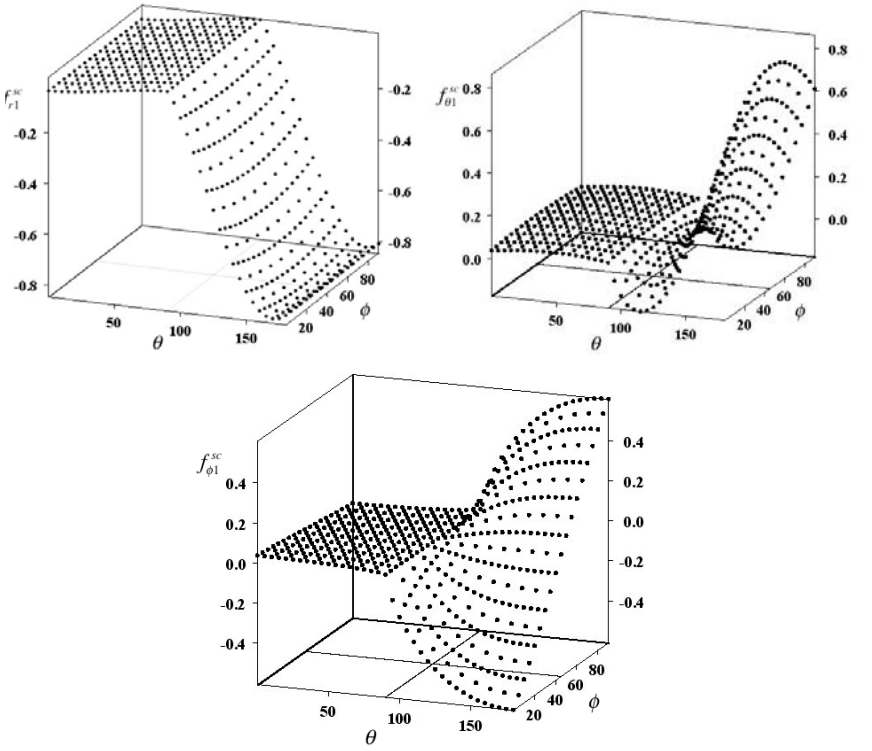

Figure 10: Distribution of angular variation of displacement fields f_{ij}^{sc} on the θ-ϕ plane in spherical coordinates

identified to be the same as those in the paper of Koguchi (2006) in order to compare the difference of the intensity of stress singularity with each other. The briefly explanation of Koguchi (2006) is described. The BEM model is shown in Fig. 7. A symmetrical of three layers bonded structure is used for BEM analysis. Figure 11 shows the stress $\sigma_{\theta\theta}/\sigma$ profile at ϕ =π/4 and θ =π/2 versus r/L for intensity of stress singularity estimation by fitting curve with the following equation.

$$\frac{\sigma_{\theta\theta}}{\sigma} = K_{\theta\theta 0} + K_{\theta\theta 1}\left(\frac{r}{L}\right)^{-\lambda} + K_{\theta\theta 2}\ln\left(\frac{r}{L}\right) + K_{\theta\theta 3}\ln\left(\frac{r}{L}\right)^{2} \tag{28}$$

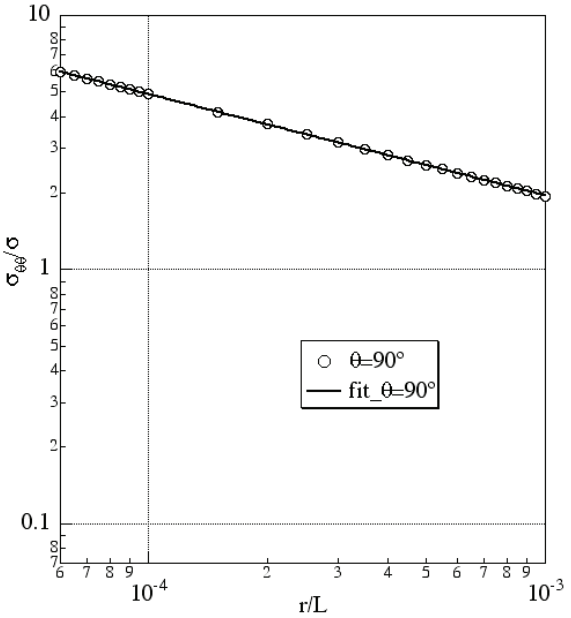

Figure 11: Stress $\sigma_{\theta\theta}/\sigma$ versus r/L for intensity of stress singularity estimation (L=10 mm.)

The results of the intensity of stress singularity $K_{\theta\theta 1}$ at ϕ =π/4 and θ =π/2 is 0.1241.

6 3D enriched FEM results and discussion

The intensities of stress singularity at singularity corner (θ =π/2 and ϕ =π/4) and singularity lines (θ =π/2) in the dissimilar material joints with a large difference of Young's moduli are determined using three-dimensional enrich FEM analysis.

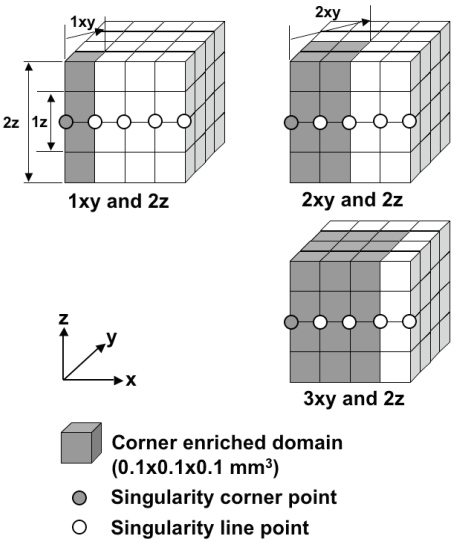

Figure 12: The increasing the singularity corner enriched domain for 0.1 mm of element size (example)

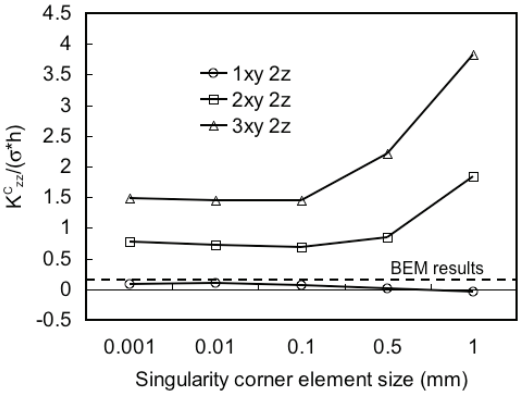

Figure 13: The K^c_{zz} results versus the singular corner element size

Many cases of the element sizes near the singular points and the enriched domains are analyzed to improve the accuracy of the intensity of stress singularity.

At first, the elements near the singularity corner are divided to small elements of all equal sized hexahedron elements. The various sizes of those elements associated with increasing of the singularity corner enriched domain in x, y directions upper

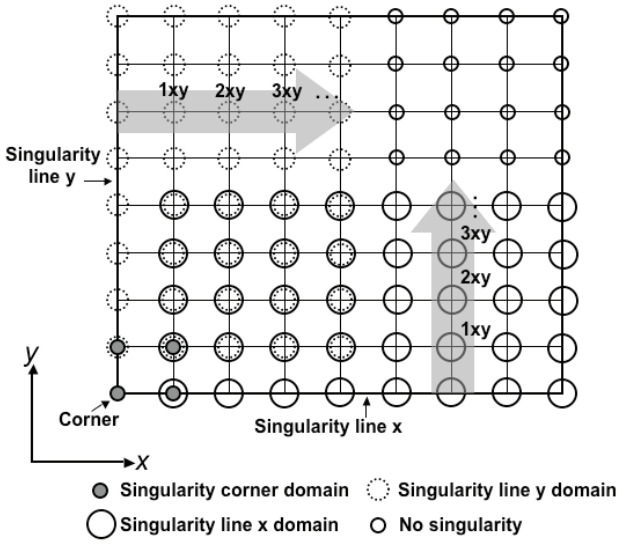

Figure 14: The influence of the singularity line enriched domain in x-y plane

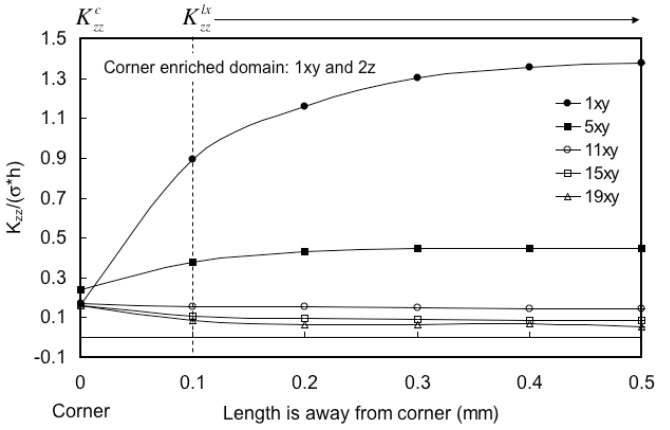

Figure 15: The results of the influence of the singularity line enriched domain in x-y plane

and lower materials, are determined. The increasing of the singularity corner enriched domain for 0.1 mm of element size are shown in Fig. 12. The results are shown in Fig. 13.

Figure 12 shows that when the corner enriched element size is equal or smaller than 0.1 mm, the results of K^c_{zz} are nearly the same with each other in each case of

the corner enriched domain. Hence, the 0.1 mm of element size can be used for improving the accurate results and the small singularity corner enriched domain gave the K_{zz}^{c} results near to the $K_{\theta\theta 1}$ results using BEM analysis. Generally, at the plane ($\theta = \pi/2$), the stress σ_{zz} in a Cartesian coordinate is the same as the stress $\sigma_{\theta\theta}$ in a spherical coordinate.

After that, the influence of the singularity line enriched domain is analyzed as the Fig. 14. The case of 1xy of the singularity corner enriched domain associated with equal increasing of the singularity line enriched domains in the perpendicular with singularity lines *x* and *y* is shown in Fig. 14. The results of *1xy-2z* of the singularity corner enriched domain associated with increasing of the singularity line enriched domains (*1xy-2z* to *19xy-2z*) are shown in Fig. 15.

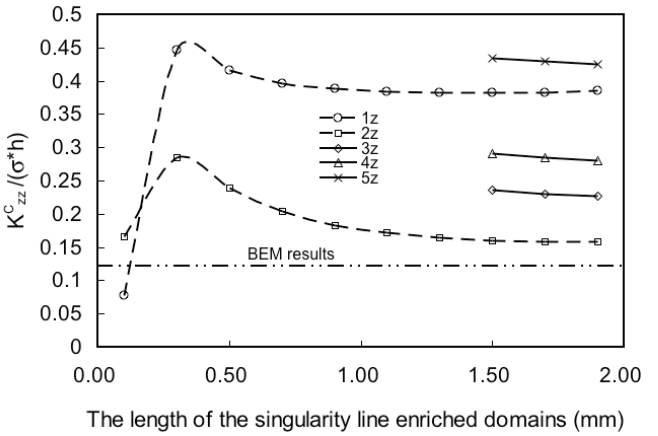

Figure 16: The influence of the singularity line enriched domain in *x*-*y* plane in various enriched domains in *z*-direction

Then, the increasing of the singularity corner and line enriched domains in *x*, *y* and *z* directions is analyzed. The results of K_{zz}^{c} are shown in Fig. 16 and if the results of K_{zz}^{c} are plotted only in the case of the singularity line enriched domain is 1.5 mm. (*15xy*), the results of K_{zz}^{c} can be shown in Fig. 17.

The increasing of the singularity line domains in *x*-*y* plane give the results of K_{zz}^{c} at singularity corner and the influence of the singularity line domains become stable, see Figs. 15 to 17. Then, the increasing of the singularities corner and line enriched domains in *z* direction to 0.4 mm (2*z*) give the results of K_{zz}^{c} near to the BEM results. Consequently, the result of K_{zz}^{c} at the singularity corner in dissimilar material joint is 0.158 under the singularity corner enriched domain is $1xy-2z$ and the singularity line enriched domains are larger than $15xy-2z$. It can be summarized that

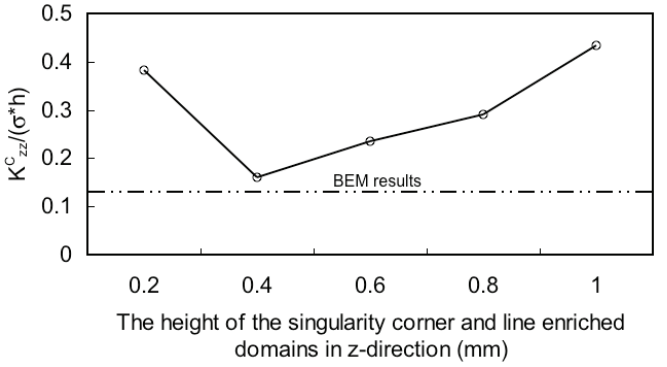

Figure 17: The results of K^c_{zz} when the singularity corner and line enriched domains increase

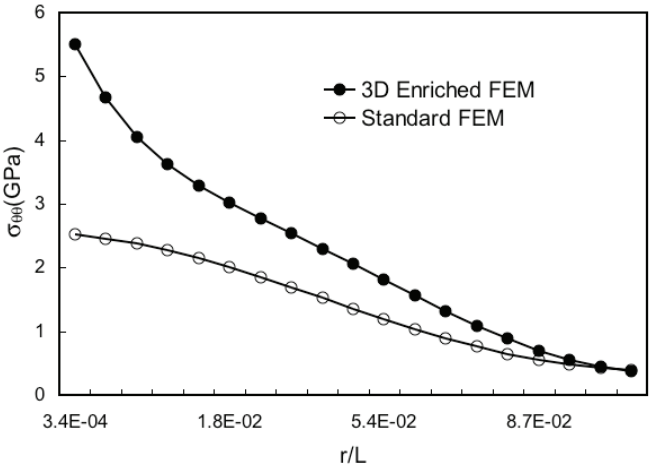

Figure 18: The stress $\sigma_{\theta\theta}$ profile near the corner singular point at $\phi = \pi/4$ and $\theta = \pi/2$

the intensity of stress singularity can be determined under the small of singularity corner enriched domain and the large of singularity line enriched domains in *x*-*y* plane. The result of K^c_{zz} in the three-dimensional enriched FEM analysis is larger than the result of $K_{\theta\theta 1}$ in the BEM analysis about 27.3 %. It may be caused from the influence of the intensities of stress singularity along the singularity lines when the value of K^c_{zz} was determined by the three-dimensional enriched FEM. Finally, the stress $\sigma_{\theta\theta}$ profile near the singularity corner at $\phi = \pi/4$ and $\theta = \pi/2$ obtained from the three-dimensional enriched FEM is compared with that obtained from the

standard FEM as shown in the Fig. 18.

Normally, stress singularity fields at a vertex can be expressed by using the standard FEM with very small elements around the vertex. However, the addition of the singular displacement fields into the FEM formulation for enriched element can express the stress singularity fields at the singularity corner even if the element is not small enough, see Fig. 18.

7 Conclusion

In the present paper, the new three-dimensional enriched FEM formulation at the singularity corner was presented. Angular functions for singularities corner and lines were derived from eigen analysis using a finite element method. The value of the intensity of stress singularity at singularity corner effecting by the intensities of stress singularity along the singularity lines, was determined and compared with that value using a boundary element method.

References:

Aksentian, O. K. (1967): Singularities of the stress-strain state of a plate in the neighborhood of an edge. *PMM,* vol. 31, no. 1, pp. 178-186.

Apel, T.; Leguillon, D.; Pester, C.; Yosibash, Z. (2008): Edge singularities and structure of the 3-D Williams expansion. *C R Mecanique,* vol. 336, pp. 629-635.

Atluri, S. N.; Zhu, T. (1998): A new meshless local Petrov-Galerkin (MLPG) approach in computational mechanics. *Computational Mechanics*, vol. 22, pp. 117-127.

Atluri, S. N.; Zhu, T. (2000): The meshless local Petrov-Galerkin (MLPG) approach for solving problems in elasto-statics. *Computational Mechanics*, vol. 25, pp. 169-179.

Atluri, S.N.; Shen, S. (2002): The meshless local Petrov-Galerkin (MLPG) method: A simple & less-costly alternative to the finite element and boundary element methods, *CMES: Computer Modeling in Engineering and Sciences*, vol. 3, no. 1, pp. 11-52.

Atluri, S.N.; Han, Z.D.; Shen, S. (2003): Meshless local Petrov-Galerkin (MLPG) approaches for solving the weakly-singular traction & displacement boundary integral equations, *CMES: Computer Modeling in Engineering and Sciences*, vol. 4, no. 5, pp. 571-586.

Atluri, S.N. (2004a): The meshless method (MLPG) for domain and BIE discretizations. Forsyth, GA, USA, Tech Science Press.

Atluri, S.N.; Han, Z.D.; Rajendran, A.M. (2004b): A new implementation of

the meshless finite volume method through the MLPG "mixed" approach, *CMES: Computer Modeling in Engineering and Sciences*, vol. 6, no. 6, pp. 491-514.

Atluri, S.N.; Liu, H.T.; Han, Z.D. (2005): Meshless local Petrov-Galerkin (MLPG) mixed finite difference method for solid mechanics, *CMES: Computer Modeling in Engineering and Sciences*, vol. 15, no. 1, pp. 1-16.

Atluri, S.N.; Liu, H.T.; Han, Z.D. (2006): Meshless local Petrov-Galerkin (MLPG) mixed collocation method for elasticity problems, *CMES: Computer Modeling in Engineering and Sciences*, vol. 14, no. 3, pp. 141-152.

Ayhan A. O. (2007): Stress intensity factors for three-dimensional cracks in functionally graded material using enriched finite elements, *Int J Solids Struct*, vol. 44, pp. 8579-8599.

Ayhan A. O. (2009): Three-dimensional mixed-mode stress intensity factors for cracks in functionally graded material using enriched finite elements, *Int J Solids Struct*, vol. 46, pp. 796-810.

Ayhan A. O.; Kaya A. C.; Nied H. F. (2006): Analysis of three-dimensional interface cracks using enriched finite elements, *Int. J. Fracture*, vol. 142, pp. 255-276.

Ayhan A. O.; Nied H. F. (2002): Stress intensity factors for three-dimensional surface cracks using enriched finite elements, *Int. J. Numerical Methods in Engineering*, vol. 54, pp. 889-921.

Bazent, Z. P.; Estenssoro, L. F. (1979): Surface singularity and crack propagation. *Int J Solids Struct*, vol. 15, pp. 405-426.

Belytschko, T.; Lu, Y.Y.; Gu, L. (1994): Element-free Galerkin method, *Int. J. Numerical Methods in Engineering*, vol. 37, pp. 229-256.

Benthem, J. P. (1977): State of stress at the vertex of a quarter-Infinite crack in a half-space. *Int J Solids Struct,* vol. 13, pp. 479-492.

Benthem, J. P. (1980): The quarter-infinite crack in a half-space; Alternative and additional solutions. *Int J Solids Struct,* vol. 16, pp. 119-130.

Benzley, S. E. (1974): Representation of singularities with isoparametric finite elements. *Int J Numer Methods Eng*, vol. 8, pp. 537-545.

Bogy, D. B. (1971): Two edge-bonded elastic wedges of different materials and wedge angles under surface tractions. *J Appl Mech ASME,* vol. 38, no. 2, pp. 377-386.

Bogy, D. B.; Wang, K. C. (1971): Stress singularities at interface corners in bonded dissimilar isotropic elastic materials. *Int J Solids Struct,* vol. 7, pp. 993-1005.

Dimitrov, A.; Andra, H.; Schnack, E. (2001): Efficient computation of order and mode of corner singularities in 3D-elasticity. *Int J Numer Methods Eng,* vol. 52, pp. 805-827.

Dimitrov, A.; Andra, H.; Schnack, E. (2002): Singularities near three-dimensional corners in composite laminates. *Int J Fract,* vol. 115, pp. 361-375.

Hagihara S.; Tsunori M.; Ikeda T.; Miyazaki N. (2007): Application of mesh-free method to elastic-plastic fracture mechanics parameter analysis, *CMES: Computer Modeling in Engineering and Sciences*, vol. 17, no. 2, pp.63-72.

Kawai, T.; Fujitani, Y.; Kobayashi, M. (1977): Stress analysis of the conical surface pit problem. *Proc Int Conf Fracture Mechanic and Technology,* Hong Kong, March, vol. 2, pp. 1165-1170.

Kawai, T.; Fujitani, Y.; Kobayashi, M. (1977): Analysis of singularity at the root of the surface crack problem. *Proc Int Conf Fracture Mechanic and Technology,* Hong Kong, March, vol. 2, pp. 1157-1163.

Koguchi, H. (1996): Stress singularity analysis in three-dimensional bonded structure. *Int J Solids Struct,* vol. 34, pp. 461-480.

Koguchi, H. (2006): Intensity of stress singularity fields at a vertex in three-dimensional bonded joints with an interlayer. *Trans JSME*, vol. 72, no. 724-A, pp. 2058-2065.

Leblond, J. B.; Leguillon, D. (1999): Asymptotic behavior of stress intensity factors near an angular point of a crack front. *Eur J Mech A/Solids,* vol. 18, pp. 135-145.

Leblond, J. B.; Leguillon, D. (1999): The stress intensity factors near an angular point on the front of an interface crack. *Eur J Mech A/Solids,* vol. 18, pp. 837-857.

Lee, Y.; Im, S. (2003): On the computation of the near-tip stress intensities for three-dimensional wedges via two-state M-integral. *J Mech Phys Solids,* vol. 51, pp. 825-850.

Li, Q.; Shen, S.; Han, Z.D.; Atluri, S.N. (2003): Application of meshless local Petrov-Galerkin (MLPG) to problems with singularities, and material discontinuities, in 3-D elasticity, *CMES: Computer Modeling in Engineering and Sciences*, vol. 4, no. 5, pp. 517-586.

Li, S.; Atluri, S.N. (2008): Topology optimization of structures based on the MLPG mixed collocation method, *CMES: Computer Modeling in Engineering and Sciences*, vol. 26, no. 1, pp. 61-74.

Nayroles,B.; Touzot, G.; Villon, P. (1992): Generalizing the finite element method: diffuse approximation and diffuse elements, *Computational Mechanics*, vol. 10, pp. 307-318.

Nei Y. F.; Chang S.; Fan X.K. (2007): The parallel mechanism of node-based seamless finite element method, *CMES: Computer Modeling in Engineering and Sciences*, vol. 19, no. 2, pp. 135-143.

Omer, N.; Yosibash, Z. (2008): Edge singularities in 3-D elastic anisotropic and multi-material domains. *Comput Methods Appl Mech Eng,* vol. 197, pp. 959-978.

Pageau, S. S.; Joseph, P. F.; Biggers, Jr. S. B. (1995): Finite element analysis of anisotropic materials with singular inplane stress fields. *Int J Solids Struct*, vol. 32, pp. 571-591.

Pageau, S. S.; Biggers, Jr. S. B. (1995): Finite element evaluation of free-edge singular stress fields in anisotropic materials. *Int J Numer Methods Eng*, vol. 38, pp. 2225-2239.

Pageau, S. S.; Biggers, Jr. S. B. (1996): A finite element approach to three-dimensional singular stress states in anisotropic multi-material wedges and junctions. *Int J Solids Struct*, vol. 33, pp. 33-47.

Pageau, S. S.; Biggers, Jr. S. B. (1997): Enrichment of finite elements with numerical solutions for singular stress fields. *Int J Numer Methods Eng*, vol. 40, pp. 2693-2713.

Wen-Hwa C.; Cheng-Hung C. (2005): On three-dimensional fracture mechanics analysis by an enriched meshless method, *CMES: Computer Modeling in Engineering and Sciences*, vol. 8, no. 3, pp. 177-190.

Wen P. H.; Aliabadi M. H.; Liu Y.W. (2008): Meshless method for crack analysis in functionally graded materials with enriched radial base functions, *CMES: Computer Modeling in Engineering and Sciences*, vol. 30, no. 3, pp. 133-147.

Williams, M. L. (1952): Surface stress singularities resulting from various boundary conditions in angular corner of plates under bending. *Proc First U.S. National Congress of Applied Mechanics ASME*, pp. 325-329.

Williams, M. L. (1952): Stress singularities resulting from various boundary conditions in angular corners of plates in extension. *J Appl Mech ASME,* vol. 19, p. 526.

Williams, M. L. (1957): On the stress at the base of stationary crack. *J Appl Mech ASME,* vol. 24, pp. 109-114.

Yamada, Y.; Okumura, H. (1981): Analysis of local stress in composite materials by 3-D finite element. *Proc of the Japan-U.S. Conf*, Tokyo, pp. 55-64.

Yosibash, Z.; Omer, N.; Dauge, M. (2008): Edge stress intensity functions in 3-D anisotropic composites. *Comp Science Tech,* vol. 68, pp. 1216-1224.

Zak, A. R.; Williams, M. L. (1963): Crack point stress singularities at a bi-material interface. *J Appl Mech (Brielf Notes)*, pp. 142-143.